

Geometric metasurface for multiplexing terahertz plasmonic vortices

Cite as: Appl. Phys. Lett. **117**, 171106 (2020); <https://doi.org/10.1063/5.0027950>

Submitted: 02 September 2020 . Accepted: 21 October 2020 . Published Online: 29 October 2020

XiaoFei Zang, Zhen Li, Yang Zhu, Jiong Xu, JingYa Xie, Lin Chen , Alexei V. Balakin, Alexander P. Shkurinov, YiMing Zhu , and SongLin Zhuang



View Online



Export Citation



CrossMark

Meet the Next Generation
of Quantum Analyzers

And Join the Launch
Event on November 17th



Register now



Zurich
Instruments

Geometric metasurface for multiplexing terahertz plasmonic vortices

Cite as: Appl. Phys. Lett. **117**, 171106 (2020); doi: [10.1063/5.0027950](https://doi.org/10.1063/5.0027950)

Submitted: 2 September 2020 · Accepted: 21 October 2020 ·

Published Online: 29 October 2020





View Online



Export Citation



CrossMark

XiaoFei Zang,^{1,2,a)} Zhen Li,¹ Yang Zhu,¹ Jiong Xu,¹ JingYa Xie,^{1,2} Lin Chen,^{1,2}  Alexei V. Balakin,^{3,4} Alexander P. Shkurinov,^{3,4} YiMing Zhu,^{1,2,a)}  and SongLin Zhuang¹

AFFILIATIONS

¹Terahertz Technology Innovation Research Institute, Terahertz Spectrum and Imaging Technology Cooperative Innovation Center, Shanghai Key Lab of Modern Optical System, University of Shanghai for Science and Technology, Shanghai 200093, China

²Shanghai Institute of Intelligent Science and Technology, Tongji University, Shanghai 20092, China

³Department of Physics and International Laser Center, Lomonosov Moscow State University, Leninskie Gory 1, Moscow 19991, Russia

⁴ILIT RAS—Branch of the FSRC «Crystallography and Photonics» RAS, Svyatoozerskaya 1, Shatura 140700, Moscow Region, Russia

a) Authors to whom correspondence should be addressed: xfzang@usst.edu.cn and ymzhu@usst.edu.cn

ABSTRACT

Surface plasmon polaritons carrying orbital angular momentum (OAM), namely, as plasmonic vortices, have attracted considerable attention in optical trapping, quantum information processing, and communications. The previous studies of near-field OAM are limited to generate only one single plasmonic vortex, which inevitably degrades further on-chip applications. Geometric metasurfaces, two-dimensional counterpart of metamaterials, enable the unprecedented capability in manipulating the phase, polarization, and amplitude of electromagnetic waves, providing a flexible platform in controlling plasmonic vortices. Here, we propose and experimentally demonstrate an approach to realize the multiplexing of terahertz (THz) plasmonic vortices based on geometric metasurfaces. Under the illumination of circularly polarized THz waves, multiple plasmonic vortices with identical topological charges are generated at the metal/air interface. Furthermore, the conversion from spin angular momentum to multiple plasmonic OAM, i.e., multiple plasmonic vortices with different topological charges, is also demonstrated. Geometric metasurfaces consisting of paired air-slits with different in-plane orientations are designed to demonstrate these characteristics. Our proposed approach may open an avenue for on-chip applications with increasing information capacity.

Published under license by AIP Publishing. <https://doi.org/10.1063/5.0027950>

Electromagnetic (EM) waves can carry spin angular momentum and orbital angular momentum (OAM), which are characterized by circularly polarized (CP) beams and vortex beams.¹ SAM is associated with the spin of a photon, and the SAM of CP EM waves can be $\pm\hbar$ per photon. EM waves possessing OAM, which is related to a helical phase structure, always show doughnut-shaped field distributions. Unlike SAM of CP EM waves, OAM of EM waves can have an infinite number of eigenmodes, and thus, OAM can be applied into high-capacity data transmission, communication, and data storage.^{2,3} The traditional methods for generating vortex beams are dependent on spatial light modulators,⁴ spiral phase plates,⁵ Q-plates,⁶ and computer-generated holograms.⁷ However, these approaches are limited to the bulky volume of OAM generators, which restricts the development of integrated systems and applications.

Metasurfaces, the two-dimensional counterpart of metamaterials, can accurately tailor the phase, polarization, and amplitude of EM

waves, providing an ultrathin and ultra-compact platform for developing miniaturized and integrated devices with unusual functionalities. A plethora of applications such as generalized Snell's law,^{8,9} metalens,^{10–15} spin-Hall effects,¹⁶ holograms,^{17–19} invisibility,²⁰ and nonlinear optics^{21,22} are demonstrated based on metasurfaces. Geometric metasurfaces consisting of antennas with identical shape and spatially variant orientations can implement the conversion of spin-to-orbital angular momentum, providing a connection between SAM and OAM. By carefully controlling the orientation of each antenna, the incident CP EM waves can be converted into vortex beam(s),^{23–36} Möbius strips,^{37,38} and composite vortices.^{39–41} Recently, near-field OAM associated with a plasmonic vortex has attracted considerable attention due to its potential applications in on-chip quantum information processing and communications. One method to generate plasmonic vortex is to design air-slit arrays or catenary structures with different orientations embedded in a metal film (to

generate the desired phase profile).^{42–45} The other method is related to designing spiral- and whirlpool-shaped air slits that can generate OAM because of the optical path difference along the azimuthal angle.^{46,47} However, the previous studies of near-field OAM are limited to generate only one single plasmonic vortex. Therefore, the on-chip applications are inevitably constrained when multiple plasmonic vortices are needed. Here, we propose and experimentally demonstrate an approach to design desired geometric metasurfaces for multiplexing THz plasmonic vortices. For the incidence of CP THz waves, multiple plasmonic vortices with identical/different topological charges are generated at the metal/air interface. The unique approach for generating multiple plasmonic vortices may open a window in manipulating SPPs and designing multifunctional on-chip devices.

Figure 1 shows the schematic of the multiplexing of near-field OAM. A geometric metasurface consisting of orthogonally distributed air-slits with different in-plane orientations is designed to generate the desired phase profile. Under the illumination of CP THz waves, the circular-shaped geometric metasurface can excite multiple plasmonic vortices with a helical wavefront. As shown in Fig. 1, two plasmonic vortices with identical topological charges (or different topological charges) can be obtained just by rotating each air-slit. Therefore, the multiplexing of plasmonic vortices is dependent on the modulation of the pure geometric phase, and thus, the corresponding metasurfaces are defined as geometric metasurfaces.

The detailed structure parameters of air-slits are $w = 130 \mu\text{m}$, $l = 300 \mu\text{m}$, $\rho' = 4104 \mu\text{m}$, and $d_1 = d_2 = \lambda_{spp}/2 \approx 342 \mu\text{m}$ [see Fig. 2(a)]. $\lambda_{spp} = \lambda \sqrt{\frac{\epsilon_d + \epsilon_m}{\epsilon_d \epsilon_m}}$ represents the SPP wavelength, and $\lambda = 684 \mu\text{m}$ is the incident wavelength. ϵ_d and ϵ_m are the permittivity of air and metal, respectively. For one air slit embedded in the metal film, the excited SPPs (under the illumination of CP THz waves) can be approximately considered as an in-plane dipole [see Fig. 2(b)]. The corresponding electric-field distribution in point p can be written as

$$E_z = e^{-\kappa_a z} A(\theta') e^{\pm i\phi(\theta')} e^{ik_{spp}|\rho - \rho'|}, \quad (1)$$

where $\phi(\theta') = \phi(\theta) - \theta'$. ρ is the distance between point p and the origin of coordinates (point O). κ_a is the attenuation coefficient.

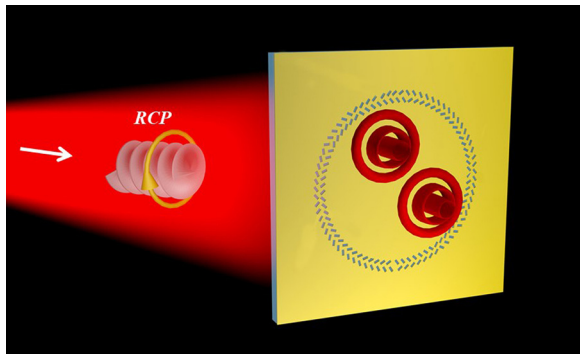


FIG. 1. Schematic of the multiplexing of plasmonic vortices: under the illumination of RCP THz waves, two plasmonic vortices are generated on the interface between air and gold film.

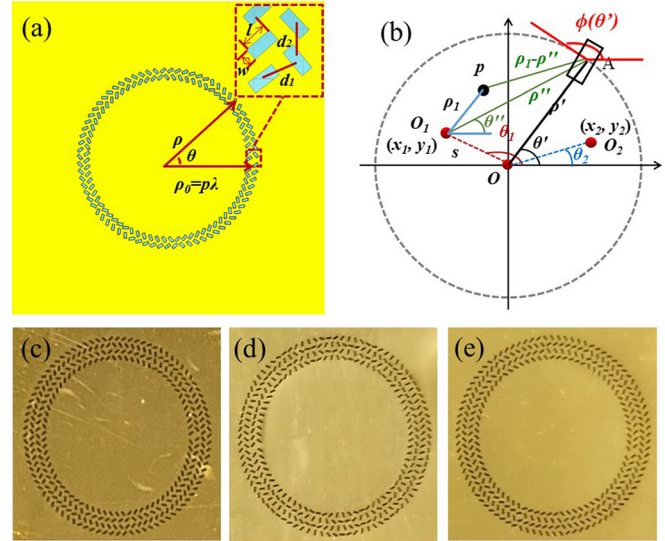


FIG. 2. (a) Structure of the geometric metasurface for generating multiple plasmonic vortices. (b) Schematic for exciting SPPs based on an air-slit. (c)–(e) The optical images of designed geometric metasurfaces for generating two plasmonic vortices with topological charges of +1, +1 (c), +2, +2 (d), and +2, +1 (e).

When circular-shaped air-slit arrays are embedded in the metal film [see Fig. 1(b)]. The total electric-field distribution at point p can be illustrated as

$$E_z = e^{-\kappa_a z} \int (A(\phi'_{in}) e^{\pm i\phi(\theta'_{in})} + A(\phi'_{out}) e^{\pm i\phi(\theta'_{out})} e^{\pm ik_{spp} \frac{\lambda_{spp}}{2}}) \times e^{ik_{spp}|\rho - \rho'|} d\theta' = e^{-\kappa_a z} \int A_0 e^{\pm i(2n-1)\theta'} e^{ik_{spp}|\rho - \rho'|} d\theta' \propto J_{\pm(2n-1)}(k_{spp}\rho'), \quad (2)$$

where $\phi(\theta') = \phi(\theta) - \theta'$. ρ is the distance between point P and point O . According to Eq. (2), a plasmonic vortex with the topological charge of $\pm(2n-1)$ is excited in the origin of coordinates. n is the slit-rotation factor that is defined as the ratio between the rotation angle of the slit in a turn and 2π . “ \pm ” is determined by the chirality of the incident CP THz waves.

For generating a plasmonic vortex at position $O_1(x_1, y_1)$, the corresponding electric-field distribution at point p can be illustrated as

$$E_z = e^{-\kappa_a z} \int (A(\phi'_{in}) e^{\pm i\phi_{in}(\theta''_{in})} + A(\phi'_{out}) e^{\pm i\phi_{out}(\theta''_{out})} e^{\pm ik_{spp} \frac{\lambda_{spp}}{2}}) \times e^{ik_{spp}|\rho_1 - \rho''|} d\theta'' = e^{-\kappa_a z} \int A_0 e^{\pm i(2n-1)\theta''} e^{ik_{spp}|\rho_1 - \rho''|} d\theta'' \propto J_{\pm(2n-1)}(k_{spp}\rho_1), \quad (3)$$

where $\rho_1 = \sqrt{(x-x_1)^2 + (y-y_1)^2}$ and $\theta'' = \arctan \frac{y-y_1}{x-x_1}$. In addition, the rotation angles of the air-slits are $\theta''_{in} = \theta''_{in} = n\theta'$ and $\theta''_{out} = \theta''_{out} = n\theta' + \pi/2$.

For multiple plasmonic vortices, i.e., two plasmonic vortices at o_1 and o_2 , the electric field distribution at point p can be illustrated as

$$\begin{aligned}
 E_z &= e^{-\kappa_a z} \int \left(A(\varphi'_{in}) e^{\pm i\phi_{in}(\theta''_1)} + A(\varphi'_{out}) e^{\pm i\phi_{out}(\theta''_2)} e^{\pm ik_{spp} \frac{\lambda_{spp}}{2}} \right) \\
 &\quad \times e^{ik_{spp} |\rho_1 - \rho''|} d\theta' + e^{-\kappa_a z} \int \left(A(\varphi'_{in}) e^{\pm i\phi_{in}(\theta''_1)} \right. \\
 &\quad \left. + A(\varphi'_{out}) e^{\pm i\phi_{out}(\theta''_2)} e^{\pm ik_{spp} \frac{\lambda_{spp}}{2}} \right) e^{ik_{spp} |\rho_2 - \rho''|} d\theta' \\
 &= e^{-\kappa_a z} \left(\int A_0 e^{\pm i(2n_1 - 1)\theta''_1} e^{ik_{spp} |\rho_1 - \rho''|} d\theta' \right. \\
 &\quad \left. + \int A_0 e^{\pm i(2n_2 - 1)\theta''_2} e^{ik_{spp} |\rho_2 - \rho''|} d\theta' \right) \\
 &\propto J_{\pm(2n_1 - 1)}(k_{spp} \rho_1) + J_{\pm(2n_2 - 1)}(k_{spp} \rho_2), \quad (4)
 \end{aligned}$$

where $\rho_2 = \sqrt{(x - x_2)^2 + (y - y_2)^2}$, $\theta''_1 = \arctan \frac{y - y_1}{x - x_1}$ and $\theta''_2 = \arctan \frac{y - y_2}{x - x_2}$.

The required phase profile of the metasurface is governed as follows:

$$\begin{aligned}
 \Phi(\theta') &= \arg \left\{ \exp \left[\frac{2\pi}{\lambda} * \left(\rho + s_1 - \sqrt{\rho^2 + s_1^2 - 2\rho s_1 \cos(\theta' - \theta_1)} \right) \right. \right. \\
 &\quad \left. \left. + (2n_1 - 1) * \theta' \right] \right. \\
 &\quad \left. + \exp \left[\frac{2\pi}{\lambda} * \left(\rho + s_2 - \sqrt{\rho^2 + s_2^2 + 2\rho s_2 \cos(\theta' - \theta_2)} \right) \right. \right. \\
 &\quad \left. \left. + (2n_2 - 1) * \theta' \right] \right\} \quad (5)
 \end{aligned}$$

where S_1 and S_2 are the distances of the two plasmonic vortices away from the origin of coordinates. The topological charges of these two vortices are $2n_1 - 1$ and $2n_2 - 1$, respectively.

To experimentally demonstrate the multiplexing of plasmonic vortices, we fabricate three samples to generate two plasmonic vortices with topological charges of +1 and +1 [see Fig. 2(c)], +2 and +2 [see Fig. 2(d)], +2 and +1 [see Fig. 2(e)], respectively. It should be noticed that dual-turn distributed air-slit arrays (each turn consisting of circular-distributed of pair air-slit arrays) were designed to demonstrate the multiplexing of plasmonic vortices, since the multi-turn design will enable stronger field enhancement than that of the single-turn. In addition, the designed structures [see Figs. 2(c)–2(e)] can only excite the E_z -component of plasmonic vortices, and the other components (E_x - and E_y -components) can be neglected. The distance between two turns was λ_{spp} . Conventional photolithography and magnetron sputtering coating were utilized to fabricate these samples. A polyimide film with a thickness of 25 μm and a permittivity of $\varepsilon = 3.5 + 0.035i$ was selected as a substrate. A layer of gold film with a thickness of 0.2 μm (and with pre-designed air-slits) was coated on one surface of the substrate. In experiment, a near-field scanning THz microscopy system (NSTMs) was utilized to detect the electric field distributions as well as phase distributions of the designed samples under the illumination of right-hand circularly polarized (RCP) THz waves. The samples were fixed, while the THz tip mounted on a translation stage was located closed to the samples to collect spatial electric field distributions.

As a feasibility study, a geometric metasurface that can generate two plasmonic vortices with topological charges of +1 and +1 in the anti-diagonal direction is demonstrated, as shown in Fig. 3. The slit-rotation factor is $n_1 = n_2 = 1$. For the incidence of right-hand

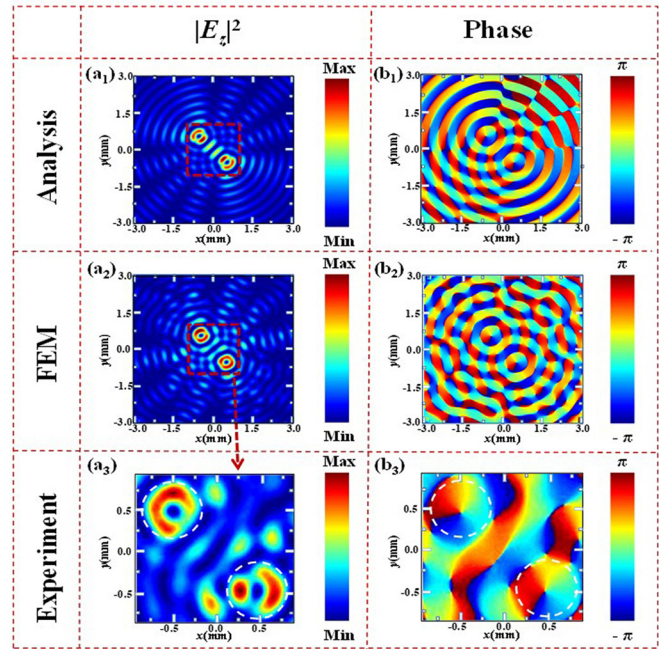


FIG. 3. (a₁) and (b₁) Analysis, (a₂) and (b₂) numerical, and (a₃) and (b₃) measured results of the electric field and phase distribution of THz plasmonic vortices with $n_1 = n_2 = 1$.

circularly polarized (RCP) THz waves, the topological charges of these two plasmonic vortices are +1 and +1. In this paper, the multiple plasmonic vortices are excited under the illumination of RCP THz waves [for left-hand circularly polarized (LCP) incidence, the theoretical model and numerical calculations of the multiplexing of plasmonic vortices are supplied in the [supplementary material](#), Sec. I]. According to Eq. (4), the excited SPPs can be analytically expressed as $J_{+1}(k_{spp} \rho_1) + J_{+1}(k_{spp} \rho_2)$, which corresponds to two +1-order Bessel functions. Figure 3(a₁) shows the analytical electric field distribution ($|E_z|^2$). There are two doughnut-shaped plasmonic vortices observed in the anti-diagonal direction. One plasmonic vortex is located at $A(-484 \mu\text{m}, 484 \mu\text{m})$, while the other one is placed at $B(484 \mu\text{m}, -484 \mu\text{m})$. The corresponding phase distribution of such a geometric metasurface is shown in Fig. 3(b₁). The overall phase change is 2π around points A and B. The numerical calculations are carried out based on the finite-element method (FEM), as shown in Figs. 3(a₂) and 3(b₂). Two plasmonic vortices are observed under the illumination of RCP THz waves [see Fig. 3(a₂)], and the spatial helical phase structures in the anti-diagonal direction reveal the topological charge (+1) of the vortices [see Fig. 3(b₂)]. Figures 3(a₃) and 3(b₃) illustrate the measured electric field distribution and the corresponding phase profile, respectively. In comparison with Figs. 3(a₁)–3(a₃), the measured field distribution is well matched with the analysis model and numerical simulation. A slight discrepancy between the measurement, calculation, and analysis model can be attributed to fabrication errors and the finite number of air slits. In addition, the phase distributions in Figs. 3(b₁)–3(b₃) are matched with each other. The calculated efficiencies of the excited SPPs and plasmonic vortices are given in the [supplementary material](#), Sec. I.

To demonstrate the versatility of the proposed approach for multiplexing THz plasmonic vortices, we further study the generation of plasmonic vortices with the topological charge of +2 in the horizontal direction, as shown in Fig. 4. In this situation, the slit-rotation factor is $n_1 = n_2 = 1.5$. The excited SPPs at the metal/air interface can be approximately described as $J_{+2}(k_{SPP}\rho_1) + J_{+2}(k_{SPP}\rho_2)$. Therefore, two plasmonic vortices with the topological charge of +2 can be generated. As shown in Fig. 4(a₁), we observe two symmetrically distributed plasmonic vortices along the x -axis. A plasmonic vortex is distributed around C(-1368 μm, 0), while the other one is located around D (1368 μm, 0), respectively. Compared with the case of $n_1 = n_2 = 1$, the excited plasmonic vortices in this case ($n_1 = n_2 = 1.5$) show a larger radius of hollow fields. The phase distribution of the plasmonic vortices is shown in Fig. 4(b₁). There are two phase jumps from $-\pi$ to π , demonstrating the topological charge of +2. By carefully controlling the orientation of each air-slit in the metal film, the required phase profile [according to Eq. (5)] can be obtained. As shown in Fig. 4(a₂) for the RCP incident THz waves, two plasmonic vortices are excited, due to the modulation of the predesigned phase profile. The calculated phase distribution is illustrated in Fig. 4(b₂). In experiment, these two plasmonic vortices are measured around points C and D, as shown in Fig. 4(a₃). As illustrated in Fig. 4(b₃), the corresponding phase distribution across a turn is 4π . It can be concluded that the topological charge of the plasmonic vortices can be well modulated by parameters of n_1 and n_2 , respectively.

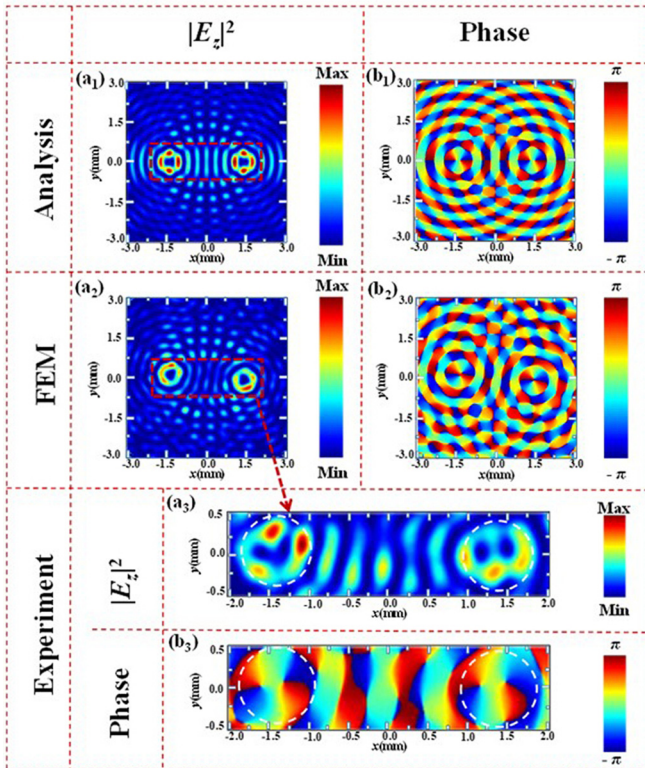


FIG. 4. (a₁) and (b₁) Analysis, (a₂) and (b₂) numerical, and (a₃) and (b₃) measured results of the electric field and phase distribution of THz plasmonic vortices with $n_1 = n_2 = 1.5$.

Our approach can not only excite the SPPs to form multiple plasmonic vortices with identical topological charge but also harness the incident CP THz waves into plasmonic vortices with different topological charges. Figure 5(a₁) shows the electric field distribution based on the analytical mode [see Eq. (4)]. Here, the slit-rotation factors are $n_1 = 1.5$ and $n_2 = 1$, respectively. Two plasmonic vortices with different radii are located around E (-2052 μm, 0) and F (0, 0), respectively. The phase distribution in Fig. 5(b₁) reveals that the topological charge of the left plasmonic vortex is +2, while it is +1 for the right plasmonic vortex. Figures 5(a₂) and 5(b₂) show the calculated electric field and phase distributions of the geometric metasurface with a predesigned phase profile [see Eq. (5)], under the illumination of RCP THz waves. The numerical simulations show a good agreement with the analysis model. In addition, the measured electric field distributions [see Fig. 5(a₃)] show that there are two plasmonic vortices excited around points E and F, respectively. The corresponding topological charges are +2 and +1, as shown in Fig. 5(b₃).

In fact, the proposed approach is unique and robust. It can not only generate multiple plasmonic vortices for the incidence of RCP THz waves but also excite multiple plasmonic vortices for LCP (left-hand circularly polarized) THz waves. The theoretical model (phase profile) and numerical simulations of the multiplexing of plasmonic vortices for LCP incident waves are given in the [supplementary material](#), Sec. II. This unique approach can be extended to generate multiple plasmonic vortices with higher order topological charges. The

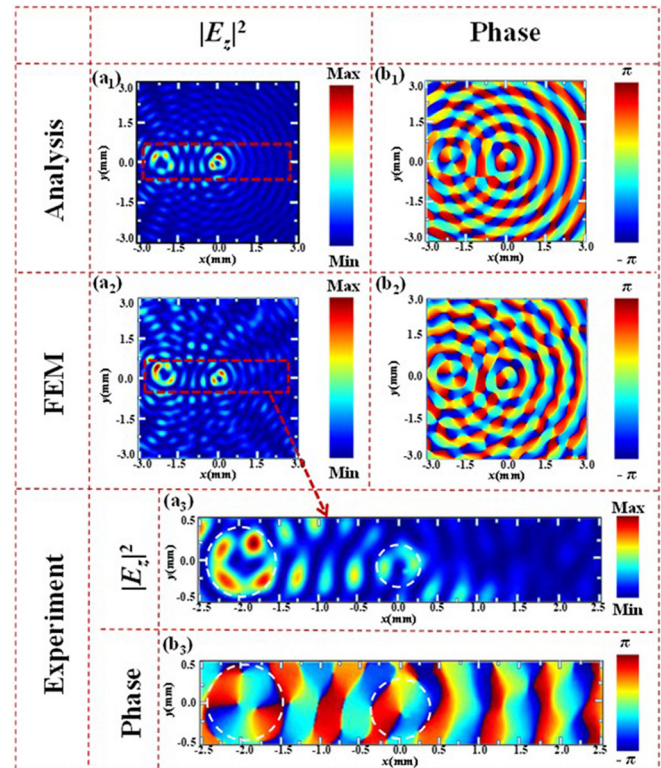


FIG. 5. (a₁) and (b₁) Analysis, (a₂) and (b₂) numerical, and (a₃) and (b₃) measured results of the electric field and phase distribution of THz plasmonic vortices with $n_1 = 1.5$ and $n_2 = 1.0$.

corresponding numerical calculations for generating two plasmonic vortices with topological charges of 3 and 4 are shown in the [supplementary material](#), Sec. III. In addition to excite two plasmonic vortices, our proposed approach can be extended to generate much more plasmonic vortices. As a proof-of-concept, the multiplexing of three and four plasmonic vortices is numerically demonstrated in the [supplementary material](#), Sec. IV. The multiplexing of plasmonic vortices with opposite sign is also numerically demonstrated in the [supplementary material](#), Sec. V.

In conclusion, we have proposed an approach to design a geometric metasurface that can excite multiple near-field vortices at the metal/air interface. The geometric metasurfaces consisting of paired air-slits with different in-plane orientations were proposed and fabricated. Under the illumination of CP THz waves, two (or more) plasmonic vortices with identical or different topological charges were observed, resulting in the multiplexing of near-field plasmonic vortices. Such a flexible approach can not only increase the information capacity of on-chip applications but also open an avenue in designing multifunctional on-chip devices.

See the [supplementary material](#) for the efficiencies of SPPs and plasmonic vortices, the multiplexing of plasmonic vortices under the illumination of LCP THz waves, the multiplexing of plasmonic vortices with higher-order topological charges, the multiplexing of multiple plasmonic vortices, and the multiplexing of plasmonic vortices with opposite sign.

This work was supported in part by the National Key Research and Development Program of China (No. 2017YFA0701005); National Natural Science Foundation of China (Nos. 61871268, 61722111, and 61705131); Natural Science Foundation of Shanghai (No. 18ZR1425600); Shanghai Pujiang Program (No. 18PJD033); “Shuguang” Program of Shanghai Education Commission (No. 19SG44); Shanghai top talent program, Shanghai international joint laboratory Project (No. 17590750300), and the 111 Project (No. D18014); the Key project supported by Science, Technology Commission Shanghai Municipality (No. YDZX20193100004960); the Russian Foundation for Basic Research under Grant Nos. 18-29-20104 and 20-21-00143; and the Ministry of Science and Higher Education in part within the Agreement No. 075-15-2019-1950 and in part within the State assignment FSRC “Crystallography and Photonics” RAS.

DATA AVAILABILITY

The data that support the findings of this study are available from the corresponding author upon reasonable request.

REFERENCES

- ¹L. Allen, M. W. Beijersbergen, R. J. C. Spreeuw, and J. P. Woerdman, *Phys. Rev. A* **45**, 8185 (1992).
- ²J. Wang, J. Y. Yang, I. M. Fazal, N. Ahmed, Y. Yan, H. Huang, Y. Ren, Y. Yue, S. Dolinar, M. Tur, and A. E. Willner, *Nat. Photonics* **6**, 488 (2012).
- ³Y. Yan, G. Xie, M. P. J. Lavery, H. Huang, N. Ahmed, C. Bao, Y. Ren, Y. Cao, L. Li, Z. Zhao, A. F. Molisch, M. Tur, M. J. Padgett, and A. E. Willner, *Nat. Commun.* **5**, 4876 (2014).
- ⁴G. Biener, A. Niv, V. Kleiner, and E. Hasman, *Opt. Lett.* **27**, 1875 (2002).
- ⁵K. Sueda, G. Miyaji, N. Miyanaga, and M. Nakatsuka, *Opt. Express* **12**, 3548 (2004).
- ⁶K. Ebrahim, B. Piccirillo, E. Nagali, L. Marrucci, and E. Santamato, *Appl. Phys. Lett.* **94**, 231124 (2009).
- ⁷N. R. Heckenberg, R. McDuff, C. P. Smith, and A. G. White, *Opt. Lett.* **17**, 221 (1992).
- ⁸N. Yu, P. Genevet, M. A. Kats, F. Aieta, J.-P. Tetienne, F. Capasso, and Z. Gaburro, *Science* **334**, 333 (2011).
- ⁹L. Huang, X. Chen, H. Mühlenbernd, G. Li, B. Bai, Q. Tan, G. Jin, T. Zentgraf, and S. Zhang, *Nano Lett.* **12**, 5750 (2012).
- ¹⁰X. Chen, L. Huang, H. Mühlenbernd, G. Li, B. Bai, Q. Tan, G. Jin, C. Qiu, S. Zhang, and T. Zentgraf, *Nat. Commun.* **3**, 1198 (2012).
- ¹¹M. Khorasaninejad, W. Chen, R. Devlin, J. Oh, A. Y. Zhu, and F. Capasso, *Science* **352**, 1190 (2016).
- ¹²R. Lin, V. Sun, S. Wang, M. Chen, T. Chung, Y. Chen, H. Kuo, J. Chen, J. Chen, Y. Huang, J. Wang, C. Chu, P. Wu, T. Li, Z. Wang, S. Zhu, and D. Tsai, *Nat. Nanotechnol.* **14**, 227 (2019).
- ¹³X. F. Zang, H. Z. Ding, Y. Intaravanne, L. Chen, Y. Peng, J. Y. Xie, Q. H. Ke, A. V. Balakin, A. P. Shkurinov, X. Z. Chen, Y. M. Zhu, and S. L. Zhuang, *Laser Photonics Rev.* **13**, 1900182 (2019).
- ¹⁴X. F. Zang, W. W. Xu, M. Gu, B. S. Yao, L. Chen, Y. Peng, J. Y. Xie, A. V. Balakin, A. P. Shkurinov, Y. M. Zhu, and S. L. Zhuang, *Adv. Opt. Mater.* **8**, 1901342 (2020).
- ¹⁵Z. R. Zhang, Q. L. Yang, M. H. Gong, M. Chen, and Z. W. Long, “Metasurface lens with angular modulation for extended depth of focus imaging,” *Opt. Lett.* **45**, 611 (2020).
- ¹⁶X. H. Ling, X. X. Zhou, X. N. Yi, W. X. Shu, Y. C. Liu, S. Z. Chen, H. L. Luo, S. C. Wen, and D. Y. Fan, *Light: Sci. Appl.* **4**, e290 (2015).
- ¹⁷G. Zheng, H. Mühlenbernd, M. Kenney, G. Li, T. Zentgraf, and S. Zhang, *Nat. Nanotechnol.* **10**, 308 (2015).
- ¹⁸D. Wen, D. F. Yue, G. Li, G. Zheng, K. Chan, S. Chen, M. Chen, K. F. Li, P. W. H. Wong, K. W. Cheah, E. Y. B. Pun, S. Zhang, and X. Chen, *Nat. Commun.* **6**, 8241 (2015).
- ¹⁹L. Jin, Z. Dong, S. Mei, Y. Yu, Z. Wei, Z. Pan, S. Rezaei, X. Li, A. Kuznetsov, Y. Kivshar, J. Yang, and C. W. Qiu, *Nano Lett.* **18**, 8016 (2018).
- ²⁰X. Ni, Z. J. Wong, M. Mrejen, Y. Wang, and X. Zhang, *Science* **349**, 1310 (2015).
- ²¹G. Hu, X. Hong, K. Wang, J. Wu, H.-X. Xu, W. Zhao, W. Liu, S. Zhag, F. Garcia-Vidal, B. Wang, P. Lu, and C.-W. Qiu, *Nat. Photonics* **13**, 467 (2019).
- ²²X. Hong, G. Hu, W. Zhao, K. Wang, S. Sun, R. Zhu, J. Wu, W. Liu, K. P. Loh, A. T. S. Wee, B. Wng, A. Alù, C.-W. Qiu, and P. Lu, *Research* **2020**, 1.
- ²³J. Lin, P. Genevet, M. A. Kats, N. Antoniou, and F. Capasso, *Nano Lett.* **13**, 4269 (2013).
- ²⁴A. Arbabi, Y. Horie, M. Bagheri, and A. Faraon, *Nat. Nanotechnol.* **10**, 937 (2015).
- ²⁵M. Pu, X. Li, X. Ma, Y. Wang, Z. Zhao, C. Wang, C. Hu, P. Gao, C. Huang, and H. Ren, *Sci. Adv.* **1**, e1500396 (2015).
- ²⁶F. Yue, D. Wen, J. Xin, B. D. Gerardot, J. Li, and X. Chen, *ACS Photonics* **3**, 1558 (2016).
- ²⁷D. Naidoo, F. S. Roux, A. Dudley, I. Litvin, B. Piccirillo, L. Marrucci, and A. Forbes, *Nat. Photonics* **10**, 327 (2016).
- ²⁸M. Mehmood, S. Mei, S. Hussain, K. Huang, S. Y. Siew, L. Zhang, T. Zhang, X. Ling, H. Liu, J. Teng, A. Danner, S. Zhang, and C. W. Qiu, *Adv. Mater.* **28**, 2533 (2016).
- ²⁹F. Yue, D. Wen, C. Zhang, B. D. Gerardot, W. Wang, S. Zhang, and X. Chen, *Adv. Mater.* **29**, 1603838 (2017).
- ³⁰L. Huang, X. Song, B. Reineke, T. Li, X. Li, J. Liu, S. Zhang, Y. Wang, and T. Zentgraf, *ACS Photonics* **4**, 338 (2017).
- ³¹R. C. Devlin, A. Ambrosio, N. A. Rubin, J. P. B. Mueller, and F. Capasso, *Science* **358**, 896 (2017).
- ³²H.-X. Xu, G. Hu, Y. Li, L. Han, J. Zhao, Y. Sun, F. Yuan, G.-M. Wang, Z. Jiang, X. Ling, T. J. Cui, and C.-W. Qiu, *Light: Sci. Appl.* **8**, 3 (2019).
- ³³W.-Y. Tsai, Q. Sun, G. Hu, P. C. Wu, R. J. Lin, C.-W. Qiu, K. Ueno, H. Misawa, and D. P. Tsai, *Adv. Opt. Mater.* **7**, 1801060 (2019).
- ³⁴H.-X. Xu, G. Hu, M. Jiang, S. Tang, Y. Wang, C. Wang, Y. Huang, X. Ling, H. Liu, and J. Zhou, *Adv. Mater. Technol.* **5**, 1900710 (2020).
- ³⁵Z. Jiang, L. Kang, T. Yue, H. Xu, Y. Yang, Z. Jin, C. Yu, W. Hong, D. Werner, and C. W. Qiu, *Adv. Mater.* **32**, 1903983 (2020).

- ³⁶Y. Bao, J. Ni, and C. W. Qiu, *Adv. Mater.* **32**, 1905659 (2020).
- ³⁷T. Bauer, P. Banzer, E. Karimi, S. Orlov, A. Rubano, L. Marrucci, E. Santamato, R. W. Boyd, and G. Leuchs, *Science* **347**, 964 (2015).
- ³⁸M. Barbuto, F. Bilotti, and A. Toscano, *IEEE Antenn. Wireless Propag.* **16**, 1345 (2017).
- ³⁹I. D. Maleev and G. A. Swartzlander, *J. Opt. Soc. Am. B* **20**, 1169 (2003).
- ⁴⁰E. J. Galvez, N. Smiley, and N. Fernandes, *Proc. SPIE* **6131**, 613105 (2006).
- ⁴¹M. Barbuto, M. Miri, A. Alù, F. Bilotti, and A. Toscano, *IEEE Trans. Antennas Propag.* **68**, 1851 (2020).
- ⁴²W. Chen, D. C. Abeyasinghe, R. L. Nelson, and Q. Zhan, *Nano Lett.* **9**, 4320 (2009).
- ⁴³N. Shitrit, I. Bretner, Y. Gorodetski, V. Kleiner, and E. Hasman, *Nano Lett.* **11**, 2038 (2011).
- ⁴⁴Q. Tan, Q. Guo, H. Liu, X. Huang, and S. Zhang, *Nanoscale* **9**, 4944 (2017).
- ⁴⁵X. F. Zang, Y. M. Zhu, C. X. Mao, W. W. Xu, H. Z. Ding, J. Y. Xie, Q. Q. Cheng, L. Chen, Y. Peng, Q. Hu, M. Gu, and S. L. Zhuang, *Adv. Opt. Mater.* **7**, 1801328 (2019).
- ⁴⁶R. Heeres and V. Zwiller, *Nano Lett.* **14**, 4598 (2014).
- ⁴⁷C. Chen, C. Ku, Y. Tai, P. Wei, H. Lin, and C. Huang, *Nano Lett.* **15**, 2746 (2015).